Relaxation dynamics in a transient network fluid with competing gel and glass phases

Pinaki Chaudhuri, Pablo I. Hurtado, Ludovic Berthier, and Walter Kob

Citation: The Journal of Chemical Physics **142**, 174503 (2015); doi: 10.1063/1.4919645
View online: http://dx.doi.org/10.1063/1.4919645
View Table of Contents: http://scitation.aip.org/content/aip/journal/jcp/142/17?ver=pdfcov
Published by the AIP Publishing

Relaxation dynamics in a transient network fluid with competing gel and glass phases

Pinaki Chaudhuri,[1] Pablo I. Hurtado,[2] Ludovic Berthier,[3] and Walter Kob[3]
[1]*The Institute of Mathematical Sciences, C.I.T. Campus, Taramani, Chennai 600 113, India*
[2]*Instituto Carlos I de Física Teórica y Computacional, and Departamento de Electromagnetismo y Física de la Materia, Universidad de Granada, Granada 18071, Spain*
[3]*Laboratoire Charles Coulomb, UMR 5221, Université Montpellier and CNRS, 34095 Montpellier, France*

(Received 29 January 2015; accepted 22 April 2015; published online 5 May 2015)

We use computer simulations to study the relaxation dynamics of a model for oil-in-water microemulsion droplets linked with telechelic polymers. This system exhibits both gel and glass phases and we show that the competition between these two arrest mechanisms can result in a complex, three-step decay of the time correlation functions, controlled by two different localization lengthscales. For certain combinations of the parameters, this competition gives rise to an anomalous logarithmic decay of the correlation functions and a subdiffusive particle motion, which can be understood as a simple crossover effect between the two relaxation processes. We establish a simple criterion for this logarithmic decay to be observed. We also find a further logarithmically slow relaxation related to the relaxation of floppy clusters of particles in a crowded environment, in agreement with recent findings in other models for dense chemical gels. Finally, we characterize how the competition of gel and glass arrest mechanisms affects the dynamical heterogeneities and show that for certain combination of parameters these heterogeneities can be unusually large. By measuring the four-point dynamical susceptibility, we probe the cooperativity of the motion and find that with increasing coupling this cooperativity shows a maximum before it decreases again, indicating the change in the nature of the relaxation dynamics. Our results suggest that compressing gels to large densities produces novel arrested phases that have a new and complex dynamics. [http://dx.doi.org/10.1063/1.4919645]

I. INTRODUCTION

In nature and in our daily life, many soft materials are formed due to the dynamical arrest of the constituent particles.[1–3] Usually they are labelled as gels if the particle density is low and as glasses if the density is large. However, the difference between these two states is at present not very well understood and therefore it is not always easy to distinguish them. Despite this difficulty, quite a few features in this glass-gel cross-cover regime have been studied extensively.

In dense glass forming liquids, the slowing down of dynamics is related to the mutual steric-hindrance in the motion of the constituent particles. The dynamical properties of these glass formers are characterized by a stretched-exponential shape of relaxation functions,[1] or similarly by the anomalous, exponential tails in the van Hove distributions of particle displacements.[4] Many of these dynamical features are described well by mode-coupling theory.[1] At even lower temperatures, the relaxation dynamics can be understood by means of the random first order transition theory.[5] In these glass formers, the structure is usually close-packed for hard sphere or van der Waals type interactions and is accompanied by a super-Arrhenius increase of viscosity. Or, if there are covalent bondings, they form network-like structures and exhibit an Arrhenius increase in viscosity.

On the other hand, chemical gels or rubbers are soft solids having random network structures.[2,6,7] The cross linking of the permanent bonds between the constituent monomers happens during the synthesis process inducing a vulcanization transition once the density of the links exceeds the percolation threshold.[8] Different static and dynamical properties in the vicinity of this transition have been studied, both using simulations and theoretical models (e.g., see Refs. 9 and 10). Physical gels are, on the other hand, low-density network structures with bonds that can be broken/realigned by thermal fluctuations within finite time scales.[7] One possible nonequilibrium path to physical gelation is via a thermal quench across the liquid-gas spinodal leading to dynamically arrested states,[11–14] that show complex aging phenomena.[15,16] In general, these paths lead to spatially heterogeneous structures. However, in recent times, considerable effort has been made to devise ways by which spatially homogeneous physical gels can be formed.[10,17–26] For such gel-forming systems, a wide variety of relaxation functions have been reported: logarithmic,[27–30] stretched,[16] or compressed exponentials.[21,31] While theoretical models[26,32–34] have been proposed to account for such dynamical properties, they are at this time certainly not yet comprehensive.

Of particular interest is the interplay between these different arrest mechanisms, viz., gel and glass, since their competition can be used to engineer materials with novel functionalities.[20,35–37] Similar studies have been carried out in systems with competing lengthscales[38,39] or interactions.[27,40,41] Yet, only few models do allow to study the low density gel phase and high density glass at the same time. Accessing this

regime is, however, necessary for investigating the structure and dynamics at those intermediate densities where the gel transforms into a glass and vice versa. Here, we study a simple three-dimensional model with direct experimental relevance,[18] and which permits us to traverse the density regime of interest and hence to study the interplay of different processes which lead to either equilibrium gelation or glassiness. Thus, our study is distinct from those addressing the competition between non-equilibrium gelation arising from arrested spinodal decomposition and glassiness.[28,37]

Furthermore, our model also allows us to tune the lifetime of bonds, a feature that is usually not present in other models (for example, see the recent work[42]). On one hand, this facilitates not only a wider exploration of the relaxation dynamics of such model physical gels, but also allows to disentangle the origin of the apparently anomalous relaxation observed in these systems. The versatility of our model, and in particular the possibility of tuning at will the bonds lifetime, allows us to explore the different mechanisms at play and hence to elucidate the interplay of various lengths and time-scales. In particular, we demonstrate that a logarithmic relaxation occurs only for specific combinations of the parameters of our model and at specific state points in the phase diagram,[20] whereas a crossover between two competing arrest mechanisms more generically yields multi-step decay of time correlation functions. This represents an instructive alternative scenario to mode-coupling theory which predicts that logarithmic relaxation may occur whenever two different arrest lines meet, one gel-like and another glass-like, and relates it to an underlying higher-order singularity in the theory.[33]

The paper is structured as follows. In Sec. II, we explain the details of our model transient-network fluid, together with the numerical schemes used to simulate its dynamics. The phase diagram of the model system and its structural properties are discussed in Secs. III and IV, respectively. In Sec. V, we analyze in detail the fluid's dynamics, quantified by the mean squared displacement and the incoherent scattering function. For that, we follow different routes across the phase diagram, which allows us to clearly understand the interplay between the gel and the glass regimes. Finally, the dynamical heterogeneities which characterise the slow dynamics in the gel and glass phases are studied in Sec. VI, followed by a summary of our results and a broader perspective in Sec. VII.

II. MODEL AND DETAILS OF SIMULATION

Our model system is a coarse-grained representation[17] of a transient gel which has been studied in experiments.[18] In this system, an equilibrium low-density gel is obtained by adding telechelic polymers to an oil-in-water microemulsion. Since the polymer end-groups are hydrophobic, the polymers effectively act as (attractive) bridges between the oil droplets they connect. The strength, lengthscale, and typical lifetime of these bridging polymers can be controlled at will. Denoting by C_{ij} the number of polymers connecting droplets i and j, we have established in Refs. 17 and 19 that the following interaction is a reasonable coarse-grained representation of this ternary system:

$$V = \epsilon_1 \sum_{j>i} \left(\frac{\sigma_{ij}}{r_{ij}}\right)^{14} + \epsilon_2 \sum_{j>i} C_{ij} V_{\mathrm{FENE}}(r_{ij}) + \epsilon_0 \sum_i C_{ii}. \quad (1)$$

The first term is a soft repulsion acting between bare oil droplets, where $\sigma_{ij} = (\sigma_i + \sigma_j)/2$, σ_i is the diameter of droplet i, and r_{ij} is the distance between the droplet centers. The second term describes the entropic attraction induced by the telechelic polymers, which has the standard "FENE" (finitely extensible nonlinear elastic) form known from polymer physics,[2] $V_{\mathrm{FENE}}(r_{ij}) = \ln(1 - (r_{ij} - \sigma_{ij})^2/\ell^2)$, and accounts for the maximal extension ℓ of the polymers. The last term introduces the energy penalty ϵ_0 for polymers that have both end-groups in the same droplet. The most drastic approximation of model (1) is the description of the polymers as effective bonds between the droplets, which is justified whenever the typical lifetime of the bonds is much larger than the timescale for polymer dynamics in the solvent.[18] Thus, for exploring the different properties of such a model, the relevant variables are the droplet volume fraction ϕ and the number of polymer heads per droplet R.[17] Note that for soft particles interacting with a continuous potential, this "volume fraction" cannot be directly compared to the one of hard spheres. In order to describe the dynamics of the system, we use a combination of molecular dynamics to propagate the droplets with interaction (1) and local Monte Carlo moves with Metropolis acceptance rates $\tau_{\mathrm{link}}^{-1} \min[1, \exp(\Delta V/k_B T)]$ to update the polymer connectivity matrix C_{ij}, where ΔV is the difference in potential energy of the system for the two bond configurations.[17,19] Thus, τ_{link} is the timescale governing the renewal of the polymer network topology. In order to prevent crystallization at high volume fractions (which would be the case for the monodisperse model studied earlier[17]), we use a polydisperse emulsion with a flat distribution of particle sizes in the range $\sigma_i \in [0.75, 1.25]$ (having a mean diameter $\sigma = 1$). The units of length, energy, and time are, respectively, σ, ϵ_1, and $\sigma\sqrt{m/\epsilon_1}$, where m is the mass of the particles. The space of control parameters is quite large. Therefore, we set $\ell = 3.5\,\sigma$ as measured in experiments,[18] $T = 1$, and $\epsilon_0 = 1$ and $\epsilon_2 = 50$, and vary the remaining parameters $\{\phi, R, \tau_{\mathrm{link}}\}$. These choices for the parameter values lead to a phase diagram which is similar to the one obtained in experiments.

Our numerical simulations are done for a three dimensional system of $N = 1000$ particles. The equations of motions of these particles are integrated using a velocity Verlet scheme with a time step of $\delta t = 0.005$. Here, most of the results are reported for $\tau_{\mathrm{link}} = 10^2$, although we also explore other values of τ_{link}: $1, 10, 10^3, 10^4$ to illustrate some of the dynamical features of the system. At each volume fraction ϕ, we first equilibrate the system of particles without any links ($R = 0$). Once equilibrated, bonds are introduced corresponding to the required value of R and then the system is again equilibrated to obtain the proper distribution of bonds per particle. Since the structure of the network is independent of the choice of τ_{link},[19] we use a small value of $\tau_{\mathrm{link}} = 1$ to expedite the equilibration process. Subsequently, data are generated by continuing the simulations with different τ_{link} values when required and the averages are typically calculated over 100 different time origins. We also do simulations for the case when the bonds between two particles are completely frozen. In order to do a proper sampling of

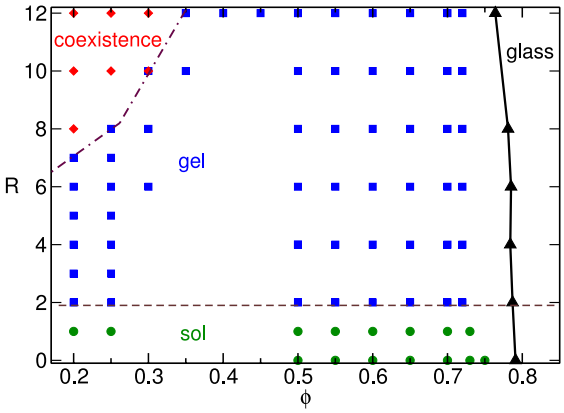

FIG. 1. Phase diagram of the system obtained by varying R and ϕ. The diamonds correspond to the coexistence region between gas and liquid, the circles to the sol phase, and the squares to the gel phase. The horizontal dashed line corresponds to onset of percolation, the dot-dashed line indicates the phase-coexistence boundary and the thick line marks the predicted glass line. Snapshots of typical configurations in each phase have been published elsewhere, see Fig. 3 in Ref. 19.

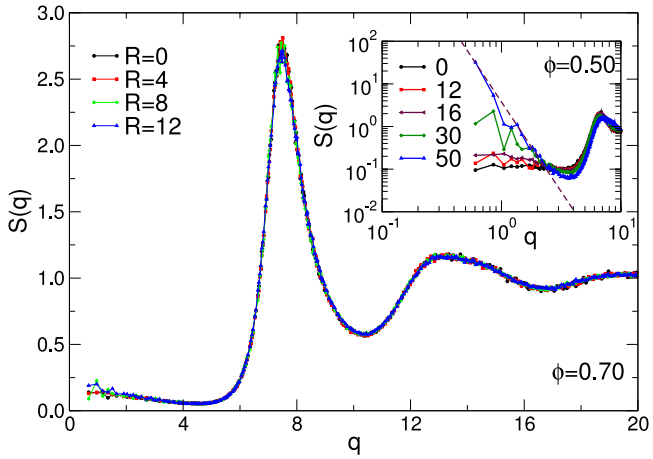

FIG. 2. Main panel: structure factor $S(q)$ computed for the particles at a volume fraction of $\phi = 0.70$ for different connectivities $R = 0, 4, 8$, and 12. Inset: $S(q)$ at $\phi = 0.50$ for $R = 0, 12, 30$, and 50. The dashed line corresponds to q^{-4}.

the network configurations for this situation, we use 6 initial configurations (positions, connectivities) from the simulations with a finite τ_{link} as initial inputs for subsequent evolution of the particle positions using molecular dynamics with the connections now permanently fixed.

III. PHASE DIAGRAM

We begin by summarizing our earlier findings for the phase diagram (shown in Fig. 1) for this model. If the number of polymers is small (i.e., $R < 2$), the system is in a simple liquid phase (the sol) at small values of ϕ. In this regime, the distribution of connectivities per particle is just an exponential.[19] With increasing ϕ, the dynamics in the sol regime becomes slow and one eventually enters a glassy phase at large ϕ, characterized by a very strong increase of the time scales for structural relaxation. If the number of bonds is large and ϕ is small, phase separation is observed due to strong attractions between the droplets. Here, the distribution of connectivities becomes bimodal, with one of the two peaks corresponding to a well-connected liquid and the other to free particles. For intermediate values of R, the system is in a gel phase. In this region of the phase diagram, the particles are connected together and form a percolating cluster and the spatial density is homogeneous. Here, the connectivity distribution is peaked around the average value and has an exponential tail. Note that this gel is an equilibrium phase since the polymer network is constantly rewired on the timescale τ_{link}. Thus, this gel formation is different from the ones obtained via the route of spinodal decomposition.[11–14] However, if we go to large enough volume fractions, we observe again a glassy system for all connectivities, with the corresponding divergence of relaxation time scales.

At low ϕ, in the gel phase, the main slow relaxation process is related to the connections between the droplets by means of the polymers and the timescale associated with its reconfiguration. At low R, as the system becomes glassy at large ϕ, the origin of the slow dynamics is the steric hindrance caused by the caging of each particle by its neighbors. In the region where both R and ϕ act as a source for slow dynamics, we have shown that the generic relaxation process has three steps but with proper tuning of the two relaxation time scales, one can also obtain logarithmic decays of the relaxation function.[20]

In the following we will discuss in detail the interplay between these two relaxation processes and show the consequences on the nature of different dynamical quantities as we move around in the phase diagram.

IV. STRUCTURE

Before we discuss the different dynamical properties of the system, we briefly look at its structure. In Fig. 2, we plot the static structure factor, $S(q)$, for a system that is dense, $\phi = 0.70$, varying the connectivity R. The general shape of $S(q)$ is very similar to the one of a simple liquid and hence, we can conclude that the system is homogeneous. Also, we see no significant dependence of $S(q)$ on R, thus showing that at high densities the structure is mainly governed by steric hindrance. For intermediate densities, however, we do note the weak dependence on R in the regime of small wave-vectors, illustrated in the inset of Fig. 2 where we show $S(q)$ for $\phi = 0.50$. This is at a volume fraction at which for large R the system approaches the coexistence region, and hence, one starts to see the emergence of a power-law behavior at small values of q with increasing R; the data for $R = 50$ can be approximated by q^{-4} (which is expected in proximity to phase co-existence[43]).

V. RELAXATION DYNAMICS

A. Dependence on volume fraction ϕ

We now characterize the dynamical properties of the system by focusing on two quantities: (i) the mean squared displacement, defined as $\Delta^2(t) = \langle \frac{1}{N} \sum_i |\mathbf{r}_i(t) - \mathbf{r}_i(0)|^2 \rangle$ and (ii) the self-intermediate scattering function, defined as $F_s(q,t) = \langle \frac{1}{N} \sum_j \exp\left(i\mathbf{q} \cdot [\mathbf{r}_j(t) - \mathbf{r}_j(0)]\right) \rangle$. Here, $\mathbf{r}_i(t)$ is the position

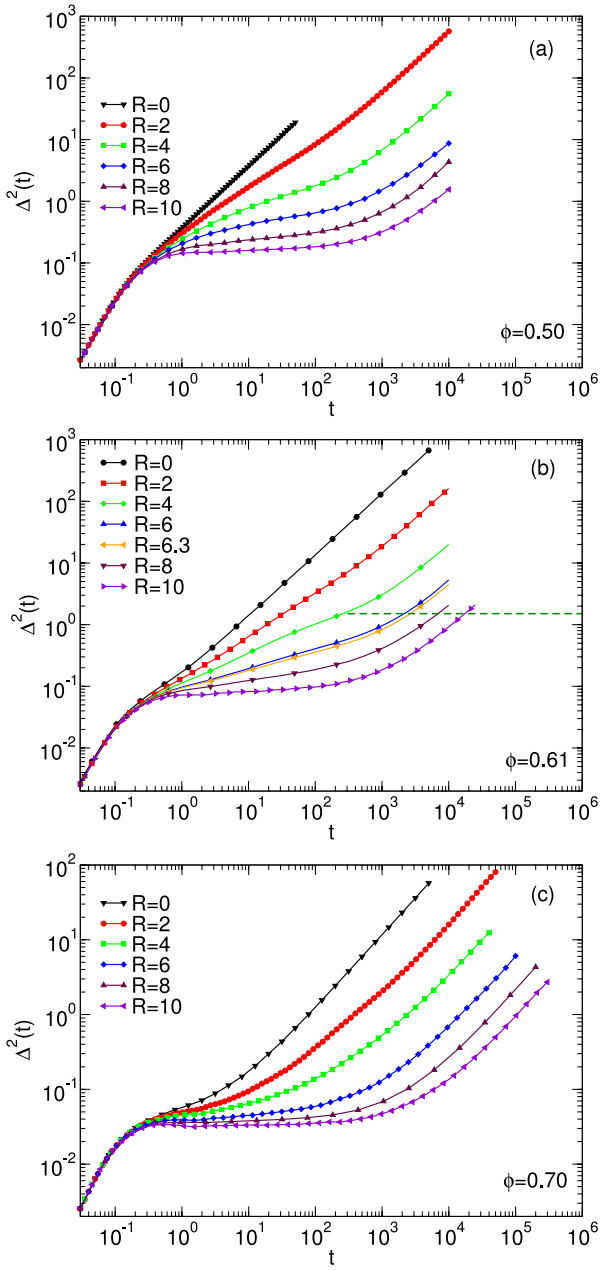

FIG. 3. Variation of mean squared displacements $\Delta^2(t)$ with changing R for (a) $\phi = 0.50$, (b) $\phi = 0.61$, and (c) $\phi = 0.70$, using a bond lifetime of $\tau_{\text{link}} = 10^2$. The dashed line marks the emergence of caging due to the bonds.

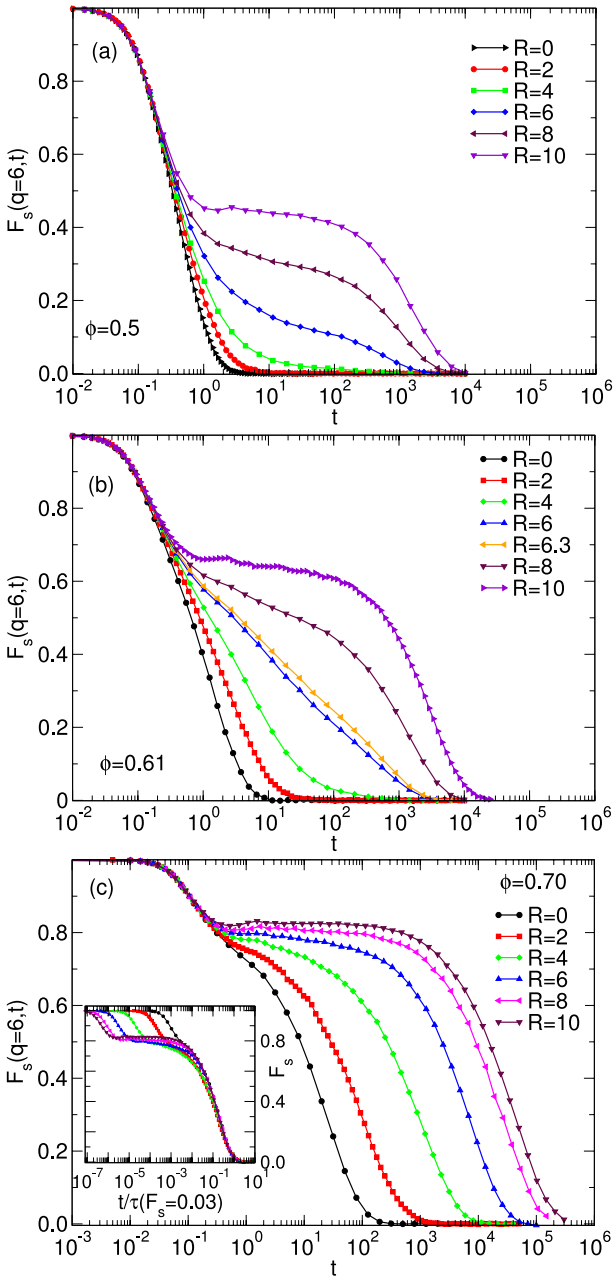

FIG. 4. Variation of the self-intermediate scattering function with changing R. (a) $\phi = 0.50$, (b) $\phi = 0.61$, and (c) $\phi = 0.70$, using $\tau_{\text{link}} = 10^2$. The inset in panel (c) shows the collapse of correlation functions for $\phi = 0.70$ after rescaling by the relaxation time, similar to time-temperature superposition principle.

of particle i at time t, q is the wave-vector, and $\langle . \rangle$ corresponds to the ensemble average.

For increasing volume fraction $\phi = 0.50, 0.61, 0.70$, we discuss simultaneously the data for $\Delta^2(t)$, shown in Fig. 3, and $F_s(q,t)$, shown in Fig. 4, computed at a wave-vector value $q = 6$. Thus, the measured $F_s(q,t)$ probes the relaxation dynamics on length scales that are slightly larger than the average particle diameter (the peak in the structure factor $S(q)$ occurs at $q \approx 7.3$).

We start in the pure gel phase ($\phi = 0.50$). The mean squared displacement, Fig. 3(a), shows that the increasing number of bonds restricts the motion of the particles: for $R > 0$ we see the emergence of an intermediate regime which develops into a well-defined plateau at $R = 10$. The height of this plateau depends significantly on R, showing that this cage motion is directly related to the transient bonds between the particles. The self-intermediate scattering function, Fig. 4(a), shows for small R a very rapid decay. This changes in that for R around 4-6, a plateau develops at intermediate and long times, the height of which depends strongly on R. The presence of this increasing plateau height, which is reminiscent of the so called type-A transition of mode-coupling theory,[33] indicates that the relaxation mechanism is changing: For small R, the motion of the particles is only weakly slowed down by the presence of the bonds, which typically break on the time scale of τ_{link}. However, for larger R, breaking a few bonds is not

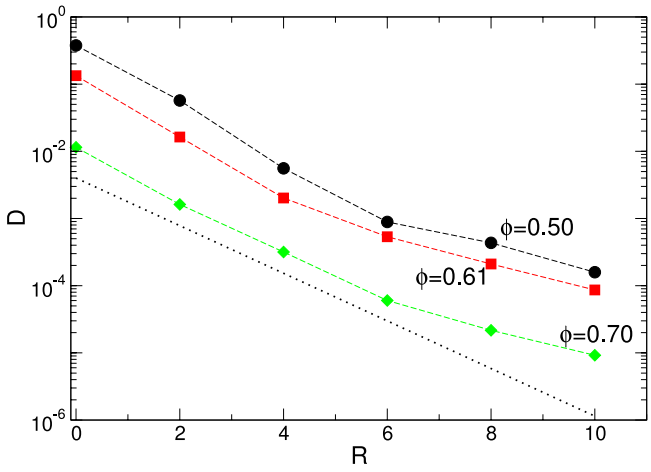

FIG. 5. Variation of diffusion constant D with R, for different ϕ (shown in Fig. 3). The dotted line, corresponding to an exponential function, is drawn as a guide to the eye.

enough to allow the particles to move since the remaining bonds still allow to maintain the particle inside its cage. Hence, this makes that at large R the relaxation dynamics does not depend very strongly on R anymore. This effect is seen in Fig. 5 where we show the diffusion constant of the particles, D, (as obtained from the mean squared displacement at long times) as a function of R. For small R, D shows a rather strong $R-$dependence, whereas for $R > 5$ this dependence becomes weaker. Below we will discuss the $R-$dependence of the relaxation time in more detail.

Next, we look at the data for an intermediate density, viz., $\phi = 0.61$, and in Fig. 3(b) we show the corresponding $\Delta^2(t)$. Like for $\phi = 0.50$, the longtime diffusion decreases with increasing R, and the $R-$dependence of the diffusion constant shows again a break at around $R \approx 5$ (see Fig. 5). For this value of ϕ we observe, however, for $R > 2$ at intermediate times, a shoulder in $\Delta^2(t)$. This shoulder, clearly visible for $R = 4$ (marked with dashed lines in Fig. 3(b)), is related to the presence of the bonds that lead to a caging of the particles on the length scale related to ℓ, the maximum extension of a bond.[44] Thus, the hint of the short-time plateau (when $\Delta^2(t) \approx 0.1$) and again one at later time (when $\Delta^2(t) \approx 1$) reflects the presence of the two different mechanisms for constraining particle motion, viz., local steric hindrance and the network bonds. Since each type of caging leads to a plateau in the intermediate scattering function,[20] the existence of the two competing mechanisms makes that at intermediate times, $F_s(q,t)$, shown in Fig. 4(b), has a very slow, almost logarithmic, decay, if R is around 6. More details on this particular case are given in the context of Fig. 11. If one compares the data for $R = 10$ at the two volume fractions $\phi = 0.50$ and $\phi = 0.61$, we recognize that the height of the plateaus in $F_s(q,t)$ increases with ϕ from which one can conclude that the proximity of the particles leads to increased tightening of the cage.

If the density is increased further to $\phi = 0.70$, the relaxation dynamics becomes strongly dominated by the steric hindrance mechanism. Already for $R = 0$ one sees a weak plateau in $\Delta^2(t)$ and its length grows rapidly with increasing R without changing much its height (see Fig. 3(c)). This is the typical behavior of simple glass-forming liquids.[45] At the same time, the self-intermediate scattering function shows the growth of a shoulder with *finite* height and this height depends again only weakly on R, Fig. 4(c). In contrast to the case at lower densities, here the shape of the correlator is basically independent of R. This is demonstrated in the inset of Fig. 4(c) where we plot $F_s(q,t)$ as a function of t/τ, with the relaxation time τ defined by $F_s(q,\tau) = 0.03$. The fact that this presentation of the curves leads to a nice master curve shows that we have for this system a time-R superposition, in analogy to the time-temperature superposition found in simple glass-forming systems.[1]

Despite the qualitative changes seen in $\Delta^2(t)$ and $F_s(q,t)$, if ϕ is increased, the $R-$dependence of the diffusion constant for $\phi = 0.70$ is very similar to the one seen at lower densities, see Fig. 5. Also for this high value of ϕ we see that this dependence is relatively strong at small R and becomes weaker if $R > 6$. Hence, the fact that at low R just few bonds have to be broken in order to allow a particle to move whereas at high R this is not a sufficient condition, is reflected in the $R-$dependence of D at *all* ϕ.

B. Varying the bond life-time τ_{link}

We will now explore further the interplay between the two processes leading to slow relaxation, i.e., the nearest-neighbor caging and the constrained motions due to the polymer bonds. Since the relative importance of these two processes depends on the lifetime of the polymer bonds, we will in the following vary this lifetime and consider values of $\tau_{\text{link}} = 10$, 10^2, and 10^3, and at fixed state-point of $R = 6.3$, $\phi = 0.61$, where logarithmic decay in the time-correlation function is observed. We study how the shape of $F_s(q,t)$ changes with varying τ_{link} and will relate this to the interplay between the two processes. This is done for different values of wave-vector in order to see how the relaxation time scales vary over different lengthscales.

We begin by looking at the case of the large $\tau_{\text{link}} = 10^3$, i.e., when the polymer bonds hinder the motion on a time scale longer than the steric hindrance effect, see Fig. 6(a). The correlation function reflects three different relaxation processes which can be seen for all values of q. Initially, the particles rattle inside the cage, resulting in partial relaxation of the correlation function on a timescale $\tau_\beta \approx 1$. Later on, the particles escape from the cage of neighboring particles (which for this value of ϕ not very pronounced) but the relaxation process is then held up by the polymer bonds. Eventually, the polymer network rewires on a timescale which is proportional to $\tau_{\text{link}} = 10^3$ and the particles start the final relaxation process. The height of the plateau in $F_s(q,t)$ increases with decreasing q, which is the typical behavior for a glassy system.[45,46] However, for the range of wave-vectors explored, the final timescale for decay of $F_s(q,t)$ depends only weakly on q. Thus, over these length scales, the relaxation process is determined by the reconfiguration of the network. However, at larger length scales, one can expect that hydrodynamic effects will eventually dominate and this will then determine the relaxation time scales.

For intermediate values of the bond lifetime, $\tau_{\text{link}} = 10^2$ in Fig. 6(b), the final decay has moved to shorter times and

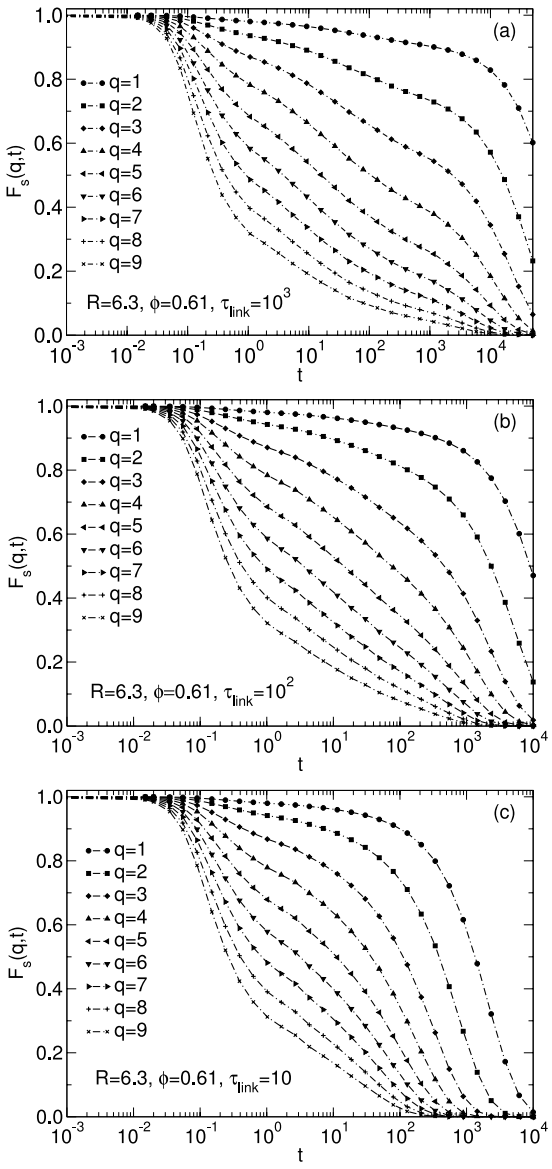

FIG. 6. $F_s(q,t)$ for $R = 6.3$, $\phi = 0.61$, (a) $\tau_{\text{link}} = 10^3$, (b) $\tau_{\text{link}} = 10^2$, and (c) $\tau_{\text{link}} = 10$.

makes that now the interplay between the two processes results in a logarithmic decay of $F_s(q,t)$ as discussed elsewhere.[20] This logarithmic dependence is seen for a range of q values (see Fig. 6(b)), with the time-window over which it exists decreasing with decreasing q. This implies that this form for the correlation function occurs only for specific combination of the relaxation time scales of the two processes of steric hindrance and eventual network relaxation. At sufficiently small q, hydrodynamic effects make the initial relaxation so slow that the second relaxation step is no longer visible and hence the logarithmic $t-$dependence is not observed any more. Finally, we mention that the logarithmic shape in the relaxation function, as discussed here, is not related to any underlying higher order mode-coupling transition, in contrast to the case of certain colloidal systems for which similar relaxation functions have been observed.[27]

If we set τ_{link} to a small value, this three-step relaxation can no longer be observed, as is seen for the case of $\tau_{\text{link}} = 10$ in the bottom panel of Fig. 6: For all q's the curve shows a (seemingly) simple two step relaxation, since the third step (related to the bonds) starts already when the second step (related to steric hindrance) is not yet completed and hence the two processes become completely mixed in time. Below we will briefly come back to this effect.

C. When the bonds are permanent

A useful way to check the influence of the polymer bonds on the relaxation dynamics is by comparing the relaxation functions for the case when the bonds are permanent, i.e., $\tau_{\text{link}} = \infty$, to those when the lifetime is finite. In Fig. 7, we do this comparison for different connectivities ($R = 4, 6$, and 8) and different values of ϕ.

In Fig. 7(a), we show $F_s(q = 6,t)$ for the case of $R = 4$ with the two different bond lifetimes $\tau_{\text{link}} = 10^2$ and $\tau_{\text{link}} = \infty$. For $\phi = 0.50$, 0.60, and 0.65, the time scales for overcoming the steric hindrance are the same for both lifetimes. However, for all ϕ, we find that the correlation function for $\tau_{\text{link}} = \infty$ shows a plateau at long times (not visible in this plot), which is due to the fact that the frozen bonds in the percolating gel-network prevent the complete relaxation of the system. In contrast, the curves for the finite τ_{link} vanish at long times. For small and intermediate ϕ the two sets of curves are very similar, indicating that the presence of a few bonds does not change the dynamics significantly. Only for $\phi = 0.7$, one sees a substantial difference in that the correlator for the permanent links decays slower than the one with $\tau_{\text{link}} = 10^2$. It is reasonable that these differences are noticeable for times somewhat longer than 10^2, i.e., the time scale of τ_{link}.

If we increase the connectivity to $R = 6$ (Fig. 7(b)), we see that the behavior is qualitatively similar to $R = 4$ in that for all values of ϕ the two curves track each other up to times around 10^2, i.e., the time of the finite τ_{link}. For larger times, the correlators for $\tau_{\text{link}} = 10^2$ decay to zero whereas the ones for $\tau_{\text{link}} = \infty$ show at long times a marked plateau. The height of this plateau depends now more strongly on ϕ than it was the case for $R = 4$, showing that if R is increased, the life time of the bonds becomes more influential. This is reasonable since it is related to the general observation that in glass-forming system small changes influence the relaxation dynamics increasingly more the slower the dynamics is. We also note that for $\phi = 0.70$, the correlator for the permanent bonds becomes very stretched. This sluggish relaxation might be related to the fact that for this value of R there are, in addition to the percolating cluster, clusters of different sizes (see Ref. 19 for typical distributions), thus giving rise to relaxation dynamics that spans many orders of magnitude in time and hence to a very stretched average correlation function. The stretching of the correlator for the frozen bonds could, however, also be due to the fact that these different clusters hinder each other resulting in the overall slowdown of the dynamics.[47]

Next, we increase the number of bonds even more, viz., $R = 8$, as shown in Fig. 7(c). We see that for the case of permanent bonds, the height of the asymptotic plateau has increased strongly in comparison to the case of $R = 6$. As a result, the correlator for $\phi = 0.70$ shows only a negligible decay of the correlation function if the bonds are permanent. The motion is so constrained by these bonds that the height of the asymptotic

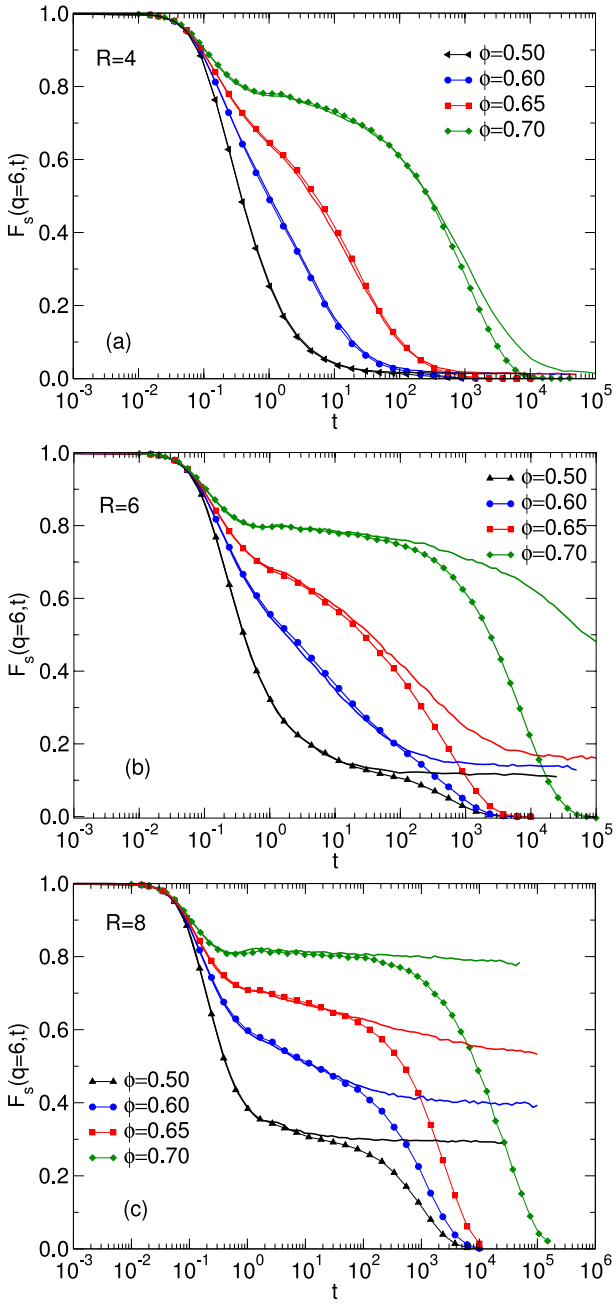

FIG. 7. $F_s(q,t)$ for different ϕ and $R = 4, 6$, and 8 when the bond lifetime is $\tau_{\rm link} = 100$ (lines with symbols) and when $\tau_{\rm link} = \infty$ (lines). The wave-vector is $q = 6.0$.

plateau, caused by the permanent bonds, becomes comparable to the one related to the steric hindrance. Also, for $\phi = 0.5$ the height of the second plateau has increased so much that the relaxation from caging is now completely masked. However, for the intermediate values of ϕ, one does notice a difference between the two plateau heights and the correlation functions decay in a very stretched fashion from one to the other. In fact, the decay is so slow that the time-dependence is seen to be logarithmic (nearly for five decades in the case of $\phi = 0.65$). Note that this logarithmic decay is due to the heterogeneous relaxation of the floppy clusters of frozen bonds, which we will discuss later in further detail. Thus, this mechanism is different from the one leading to the logarithmic relaxation seen in Fig. 4 which was due to a unique combination of the two *finite* relaxation time scales.

We now study the floppiness of this network of particles connected by the permanent bonds by probing the wave-vector dependence of the relaxation functions $F_s(q,t)$. In Figs. 8(a) and 8(b), we show for $\phi = 0.60$ the variation of $F_s(q,t)$ for $R = 2$ and 4, i.e., in the region of the phase diagram where gelation sets in. The height of the plateau at long times, also called non-ergodicity parameter, is a measure for the stiffness of the network on the length scale q considered. Comparing the two panels we recognize that, for a given q, the height of the plateau increases with increasing R. Denoting this height by $f_q^{\rm PN}$, we show in Fig. 8(c) that $f_q^{\rm PN}$ shows basically an

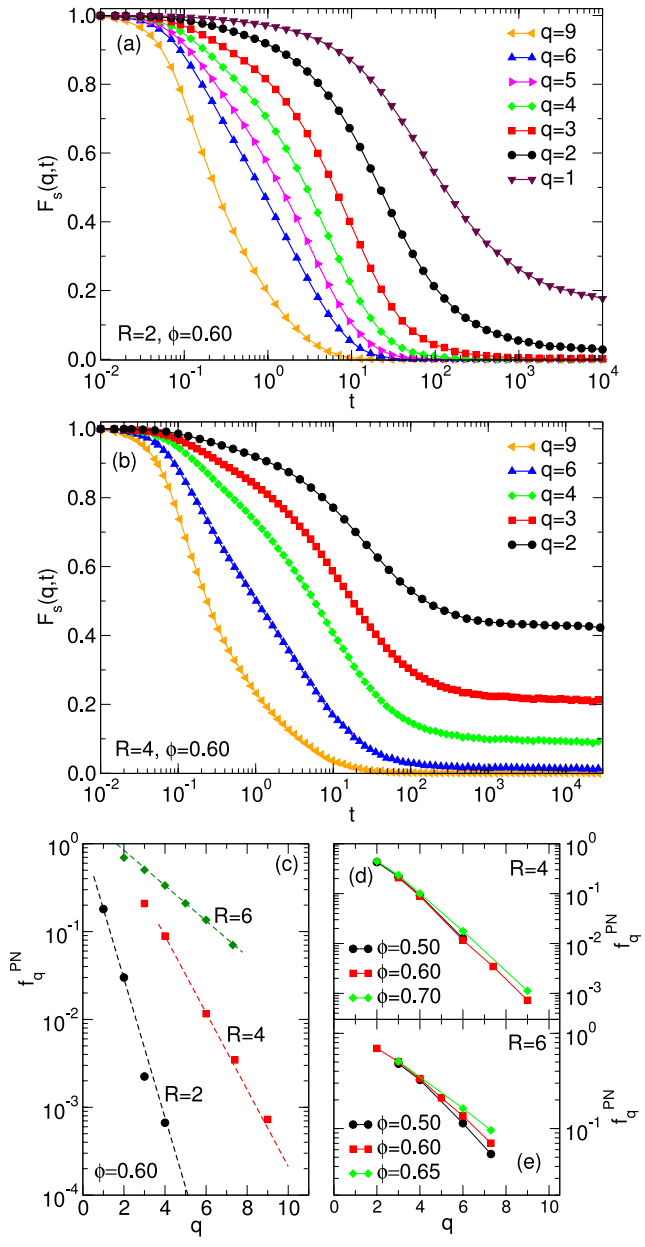

FIG. 8. (a) and (b) Variation of $F_s(q,t)$ with wave-vector q for $R = 2$ and 4 at $\phi = 0.60$ with $\tau_{\rm link} = \infty$. (c) Height of plateau, $f_q^{\rm PN}$, of $F_s(q,t)$ at long times as a function of q for $R = 2$, 4, and 6. The dashed lines are fits of the form $\exp(-q/\xi)$ with the corresponding $\xi = 0.55$, 0.99, and 2.27. (d) and (e) $f_q^{\rm PN}$ vs. q for different values of ϕ for $R = 4$ and 6.

exponential decrease in q with a slope that decreases rapidly with increasing R. That $f_q^{\rm PN}$ decreases with increasing q is of course reasonable since on small length scales the particles have more leeway to flop around than on large length scales. Note, however, that this exponential dependence is in contrast to the one found for the height of the plateau due to the steric hindrance, the latter being basically a Gaussian function.[46] Since in the representation of Fig. 8(c) such a Gaussian dependence is given by a parabola, we see that such a curve will intersect the one for $f_q^{\rm PN}$ at a certain value of q_x. For $q < q_x$ the plateau due to the steric hindrance is above $f_q^{\rm PN}$, thus making that one observes two plateaus in the correlator. However, for $q > q_x$ the plateau at long times is higher than the steric one, thus making that the latter one will be completely masked by the former and thus the correlator will show only one plateau.

We have also studied how the $q-$dependence of $f_q^{\rm PN}$ changes with the volume fraction, and in Figs. 8(d) and 8(e), we show $f_q^{\rm PN}$ for $R = 4$ and 6, respectively. For both cases, we see that the rigidity of the network at large scales, i.e., small q, is not affected by the volume fraction which is not surprising. For $R = 4$, we see that this is also true at small length scales, whereas for $R = 6$ we note a significant $\phi-$dependence if q is large. This difference is likely related to the fact that the system with $R = 6$ is much more sluggish than the one for $R = 4$, see Fig. 7, and hence small changes (here in ϕ) will have a stronger impact on the dynamics.

Finally, we disentangle the dynamics of the particles that belong to the percolating cluster from the ones that are not attached to it. In the following discussion, these are referred as clustered and non-clustered particles, respectively. The objective is to clarify the respective contributions to the different dynamical quantities that we have discussed above. We do this comparison for an increasing number of connections R at a fixed (large) volume fraction of $\phi = 0.65$. In Fig. 9, we show the data for $\Delta^2(t)$ and $F_s(q,t)$ for these two families of particles.

The mean squared displacement of the clustered particles shows, after the ballistic regime at short times, a shoulder that is related to the cage of the steric hindrance (Fig. 9(a)). This localization is, however, only temporary and is followed by a further increase of $\Delta^2(t)$. Only at longer times $\Delta^2(t)$ saturates at a height that depends on R. We note that the approach to this asymptotic height becomes increasingly slow with increasing R and in fact for $R = 8$, the time dependence is close to logarithmic and does not end within the time window of our simulation. This behavior is also seen in the self-intermediate scattering function $F_s(q,t)$ (Fig. 9(b)). At short times, the correlator decays quickly onto a plateau (not very pronounced) before the relaxation of the steric hindrance starts. For $R = 4$ and 6, this process ends in that the correlator reaches the final plateau (which is given by $f_q^{\rm PN}$ discussed above). However, for $R = 8$ the final decay is so slow, again compatible with a logarithmic time dependence, that we do not see the asymptotic behavior.

Finally, we look at the motion of the non-clustered particles and compare it with the one for $R = 0$. From Fig. 9(a), we recognize that at this volume fraction also these particles are slowed down by the cage effect in that one sees for all values of R a shoulder in $\Delta^2(t)$ at time $t \approx 1$. For $R = 0$, the $\Delta^2(t)$ shows then immediately the diffusive behavior, i.e., it is proportional to t. However, if R is increased, the $t-$dependence of $\Delta^2(t)$

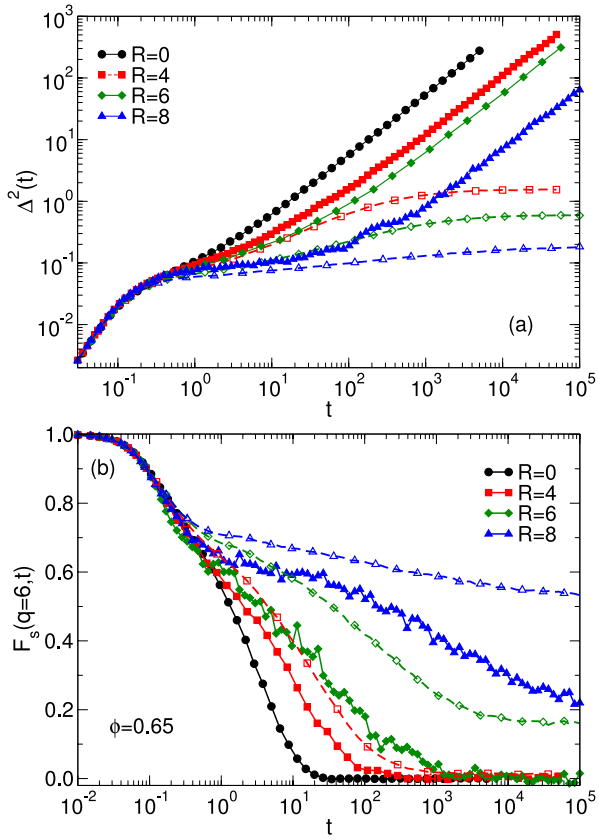

FIG. 9. Relaxation dynamics of the clustered (dashed lines with open symbols) and non-cluster particles (full lines with filled symbols) for the case of frozen bonds (i.e., $\tau_{\rm link} = \infty$), at $R = 0$, 4, 6, and 8 for volume fraction $\phi = 0.65$. (a) Mean squared displacement $\Delta^2(t)$. (b) Self-intermediate scattering function $F_s(q,t)$ for $q = 6$.

for the non-clustered particles follows first the one of the clustered particles. Only once the latter starts to reach the plateau discussed above, do the former cross over to the diffusive behavior. Hence, we can conclude that before this crossover the relaxation dynamics of the two population of particles are strongly coupled. This result is reasonable because in order to move, the non-clustered particles have to explore the holes within the percolating cluster formed by the particles which are permanently linked.

Also the self-intermediate scattering function of the non-clustered particles tracks one of the clustered particles at short times (Fig. 9(b)). However, once the latter starts to show at long times a plateau that has a significant height, the two correlators differ strongly since the one for the non-clustered particles decays to zero at long times. From the graph we also see that for $R = 8$, the correlator is extremely stretched and shows almost a logarithmic $t-$dependence. This very slow decay indicates that the mobile clusters can move around the percolating cluster only with great difficulty, a behavior that is similar to the relaxation dynamics of particles moving in random porous media.[48,49] It is also interesting that for the highest R the mean squared displacement shows for the last two decades in time a nice diffusive behavior, whereas $F_s(q,t)$ is far from having decayed to zero. This apparent contradiction is related to the fact that $\Delta^2(t)$ is dominated by the particles that move relatively fast (i.e., they are in the small clusters)

whereas $F_s(q,t)$ is dominated by the slowly moving particles (i.e., the large clusters). This cluster-size dependent dynamics leads to a so-called dynamical heterogeneity and in Sec. VI we will discuss this phenomenon in more detail.

Although we show in Fig. 9 the comparison between the dynamics of clustered and non-clustered particles for the case that $\tau_{\rm link}$ is infinitely large, it is evident that for a very large but *finite* value of $\tau_{\rm link}$, the relaxation dynamics will be very similar. Hence if, e.g., $\tau_{\rm link}$ is on the order of 10^5, basically none of the shown curves will change significantly and thus, the conclusions drawn from Fig. 9 will apply also for such value of $\tau_{\rm link}$.

D. Relaxation time scales

We now investigate how the two different relaxation time scales, one due to breaking of local cages and the other due to the reconfiguration of the network-bonds, vary with the volume fraction ϕ and the connectivity R.

To start, we consider the case of structural relaxation related to the steric hindrance. In order to avoid that this relaxation process is influenced by the one of the network, we consider the case in which the latter is completely suppressed, which can be achieved by choosing $\tau_{\rm link} = \infty$. In the following, we will study the relaxation times associated with the intermediate scattering function for wave-vector $q = 6$. As discussed above, this correlator shows at long times, an asymptotic plateau the height of which, $f_q^{\rm PN}$ depends on R and ϕ. To take this into account, we define the relaxation time $\tau_{\rm SH}$ to be the time at which $F_s(q,t) - f_q^{\rm PN} = 0.03$. The evolution of $\tau_{\rm SH}$ with ϕ is shown in Fig. 10(a), for different values of R.

We see that in the absence of any bonds, i.e., for $R = 0$, we have the usual slowing down of dynamics with increasing ϕ. The $\phi-$dependence of the relaxation time can be fitted by a Vogel-Fulcher-Tammann-law of the form $\tau_{\rm SH} \sim \exp[A/(\phi_c - \phi)^\beta]$, with $\beta \approx 1$, from which we can estimate the volume fraction ϕ_c at which the relaxation times would diverge. If we increase the number of bonds among the particles, we see that $\tau_{\rm SH}$ increases. That this increase is not just a constant ($R-$dependent) factor but depends also on ϕ is demonstrated in the inset of the figure where we have normalized the relaxation times to their1 value at $\phi = 0.5$. Using the Vogel-Fulcher-Tammann-law we can thus extract from these data the $R-$dependence of ϕ_c, which can be considered as a proxy for the $R-$dependence of the glass transition temperature. This $\phi_c(R)$ line is included in Fig. 1 as well and we see that it has a weak negative slope with $\phi_c(R = 0) = 0.847$ and $\phi_c(R = 6) = 0.808$. Thus, we can conclude that the glass transition as induced by the steric hindrance mechanism does not depend strongly on the value of R, and exhibits the characteristics of fragile glass-formers, unlike silica.[52] However, since the prefactor of the Vogel-Fulcher-law does depend strongly on R, we can conclude that a line of iso-relaxation time will bend significantly more.

Next, we investigate how the timescale for the full relaxation of the network of particles depends on the average number of bonds, R. For this, we define a relaxation time using the $t-$dependence of $F_s(q = 6,t)$ with a very short lifetime for the bonds ($\tau_{\rm link} = 1$). $\tau_{\rm PN}$ is then defined via $F_s(q = 6, \tau_{\rm PN}) = 0.03$

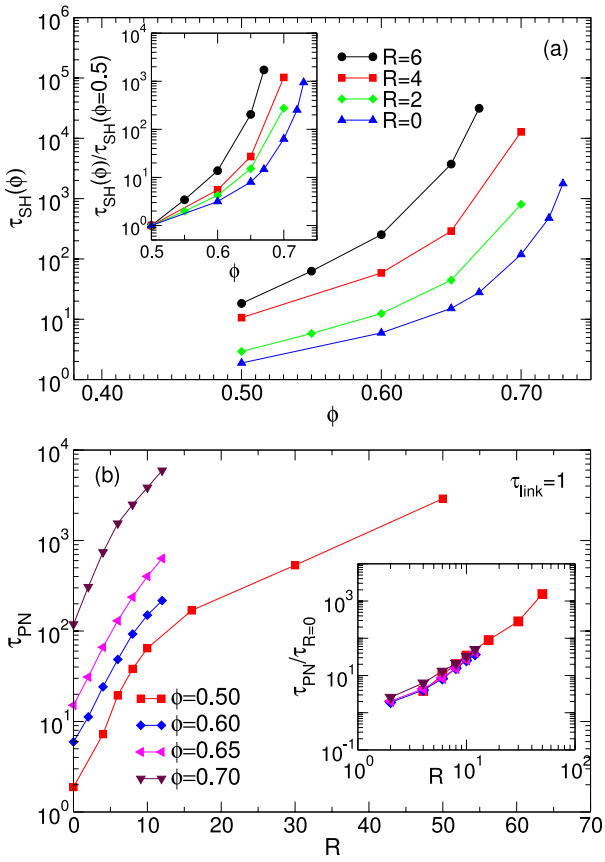

FIG. 10. (a) Main panel: plot of $\tau_{\rm SH}$ vs. ϕ for different values of R. Inset: same data scaled by $\tau_{\rm SH}(q, \phi = 0.5)$. (b) Main panel: $\tau_{\rm PN}$ vs. R, for different values of ϕ. Inset: same data as in the main panel but normalized by the relaxation time for $R = 0$, leading to a master curve. Note the double logarithmic scale in this plot.

and the $R-$dependence of this relaxation time is shown in Fig. 10(b). The figure shows that for small and intermediate values of R, the R-dependence is independent of the volume fraction in that the curves for the different values of ϕ seem to be just shifted vertically. That this is indeed the case is demonstrated in the inset where we show that a plot of the same data, but now normalized to the relaxation time for $R = 0$, gives a master curve. The main panel shows that at small concentration of bonds, the $R-$dependence is close to an exponential, a result that is likely related to the fact that increasing R leads to a tighter cage for the steric hindrance and hence a slower dynamics. However, for intermediate values of R the curve $\tau_{\rm PN}$ starts to bend over towards a weaker $R-$dependence. In order to investigate this effect better, we have carried out simulations for $\phi = 0.50$ at very high values of R: 16, 30, and 50. We find that in this regime the relaxation time follows closely an exponential (see main Fig. 10(b)), but with an exponential scale that is smaller than the one seen at small R. Note that this dependence implies that there is no singularity in the relaxation dynamics at any finite value of R, at least for this volume fraction. Instead, the dynamics shows a behavior that is similar to an Arrhenius law in that the barrier for the relaxation depends only on the number of bonds between the particles. This observation is in agreement with earlier simulations for equilibrium gels.[53]

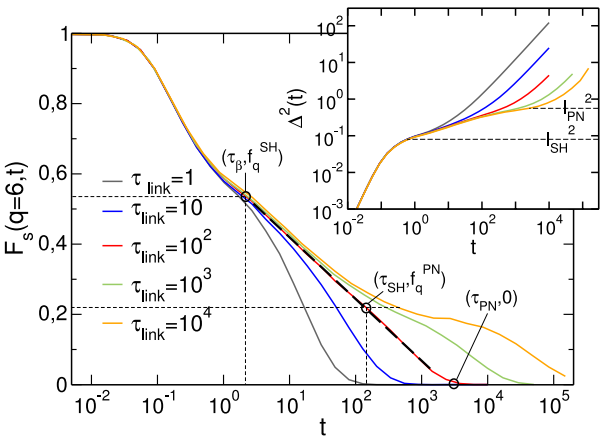

FIG. 11. $F_s(q,t)$ vs. t for $R = 6.3$, $\phi = 0.61$, and different $\tau_{\rm link}$. The inset shows $\Delta^2(t)$ for the same parameters. The dotted lines in the main figure mark the plateaus in $F_s(q,t)$: $f_q^{\rm SH}$ and $f_q^{\rm PN}$, which respectively correspond to the localization lengths $l_{\rm SH}$ and $l_{\rm PN}$ indicated in the inset.

We conclude this discussion by using the different relaxation time scales to develop a criterion that tells whether or not the correlator $F_s(q,t)$ will show the logarithmic $t-$dependence discussed in the context of Fig. 4(b). For this, we define f_q^{α} as the height of the plateau associated to the α-process, with $\alpha \in \{\rm SH, PN\}$, and recall that τ_β, $\tau_{\rm SH}$, and $\tau_{\rm PN} \propto \tau_{\rm link}$ are the time scales for the three different relaxation processes described above, namely, the rattling inside the cage, the escape from the local cage, and the network renewal process. We can now define a simple criterion for the anomalous logarithmic relaxation to be observed by requiring that the slope of the two segments defined by pairs $[(\ln\tau_\beta, f_q^{\rm SH}), (\ln\tau_{\rm SH}, f_q^{\rm PN})]$ and $[(\ln\tau_{\rm SH}, f_q^{\rm PN}), (\ln\tau_{\rm PN}, 0)]$ is the same, see Fig. 11. It is known that for glass-forming systems, the plateau related to steric hindrance is a Gaussian function of the wave-vector q, $f_q^{\rm SH} \sim \exp(-q^2\ell_{\rm SH}^2)$.[46] We showed earlier, see Fig. 8(c), that for the PN-process, $f_q^{\rm PN}$ has an exponential shape at large q (the regime corresponding to anomalous logarithmic behavior). Putting these elements together we thus obtain

$$(q\ell_{\rm PN} - q^2\ell_{\rm SH}^2) = \ln\left[1 + \frac{\ln(\tau_{\rm SH}\tau_\beta^{-1})}{\ln(\tau_{\rm PN}\tau_{\rm SH}^{-1})}\right]. \qquad (2)$$

This equation relates a purely structural observable which depends on the competition between two localization length-scales with dynamical information encoded in the different relaxation times, predicting a precise connection between structure and dynamics whenever anomalous logarithmic relaxation is to be expected.

VI. HETEROGENEITIES IN DYNAMICAL PROPERTIES

Typical glass formers show a heterogeneous dynamics of the particles when the system is increasingly supercooled. It reflects the broad distribution in the time scales for local structural relaxations.[54] On the other hand, we have reported earlier[17] that also the dynamics in the gel phase can be heterogeneous: The particles in the percolating cluster and those that are unattached have different mobilities till the time scales at which the bonds in the network are reconfigured. In the following, we will thus explore how these two different sources of heterogeneity interact as we increase the density of particles as well as the number of connectivities in the system.

We use two different measures of dynamical heterogeneity. The first one is the non-Gaussian parameter $\alpha_2(t)$, defined as $\alpha_2(t) = 3\langle r^4(t)\rangle/5\langle r^2(t)\rangle^2 - 1$, where $\langle r^2(t)\rangle$ and $\langle r^4(t)\rangle$ are the second and fourth moments of the distribution function of single particle displacements $G_s(r,t) = N^{-1}\sum_i\langle\delta(r - |\mathbf{r}_i(t) - \mathbf{r}_i(0)|)\rangle$, i.e., of the self-part of the van Hove function. A non-zero value of $\alpha_2(t)$ quantifies the extent of deviation from a Gaussian shape for $G_s(r,t)$.[50] Note that $G_s(r,t)$ is Gaussian at short times, i.e., in the ballistic regime, and again at long times when the particles are diffusive.

The second measure is the dynamic susceptibility $\chi_4(q,t)$, computed via the fluctuations of time-correlation function: $\chi_4(q,t) = N[\langle F_s^2(q,t)\rangle - \langle F_s(q,t)\rangle^2]$. It is designed to capture the spatiotemporal correlations of particle mobilities and provides, from its peak value, an estimate of the dynamic correlations.[51,54] Such functions have also been analyzed for gels with permanent bonds[55] or low density gels.[56]

A. Non-Gaussian parameter $\alpha_2(t)$

We begin by looking at how the non-Gaussian parameter varies with changing connectivities R, either when we go from the liquid to the gel phase, at $\phi = 0.50$, or when we are in a strongly glassy region, $\phi = 0.70$. For the case $\tau_{\rm link} = 10^2$, the data are shown in Fig. 12.

For $\phi = 0.50$, Fig. 12(a), $\alpha_2(t)$ shows at $t \approx 1$ a peak if $R = 0$ and a shoulder for $R > 0$. This feature is thus related to the dynamical heterogeneity due to the steric hindrance mechanism, as in usual glass-forming systems.[45] For $R > 0$ we find in addition a very prominent peak the location of which is basically independent of R, which shows that for this packing fraction the time at which the system is maximally heterogeneous does not depend on R. This observation is in tune with our earlier discussion that the timescale for structural relaxation at small values of ϕ does not change with R if the number of bonds is not very large (see Fig. 4(a)). The maximum occurs around $t \approx 10^3$, a time which corresponds to a timescale for which a significant number of particles have broken the bonds with their neighbors and exit the constraints of the network. The location of the peak is thus somewhat larger than $\tau_{\rm link}$. As has been documented in Ref. 17, at small packing fractions one has on this timescale two families of particles, one for the mobile particles and the other related to those that are immobile and as a consequence the shape of $G_s(r,t)$ deviates strongly from a Gaussian. Figure 12(a) indicates thus that the same behavior persists to the larger volume fraction of 0.50. One interesting feature is that the peak height is non-monotonous in R in that it increases till $R = 6$ and then decreases again for larger R values. The reason for the growth is that an increasing R allows for more diverse values of the connectivity for the particles, and hence to a stronger variety in the dynamical behavior. On the other hand, if R is very large most of the particles are strongly connected all the times and hence show a much smaller variation in their relaxation dynamics, i.e., they behave like in a mean-field like regime.

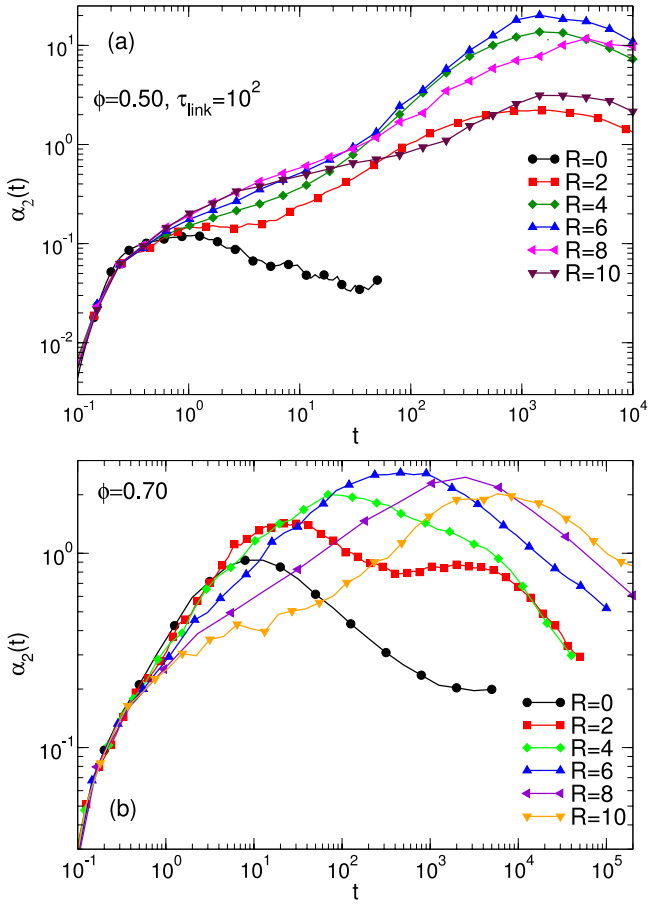

FIG. 12. Time dependence of α_2 for different values of R (as marked in the graphs) for $\tau_{\rm link} = 10^2$. (a) $\phi = 0.50$ in double-logarithmic representation and (b) $\phi = 0.70$.

Next, we study the behavior for $\phi = 0.70$, Fig. 12(b). When there are no bonds, $R = 0$, we see that $\alpha_2(t)$ is peaked at around $t = 8$. This peak, which is related to the steric hindrance, corresponds thus to the one seen for $\phi = 0.50$ at $t \approx 1$ and which, due to the higher density has shifted to larger times. For $R = 2$ (when the percolating cluster of the bonds develops), the location of this peak slightly shifts to larger times and one sees the appearance of a second peak at $t \approx 2000$ (corresponding to the time scales for renewal of the network connectivities). However, the dominant heterogeneity is still due to the local steric hindrances. As R is increased, the location of the first peak continues to shift to longer time scales, in track with the increasing structural relaxation time scales (see Fig. 4(c)), and also its height increases, in qualitative agreement with the behavior found in simple glass-formers if the coupling is increased.[45] For $R = 6$, the two peaks have merged, since the time scales for the two sources of heterogeneity are nearly the same, and thus, $\alpha_2(t)$ has a single peak. If R is increased even more, the position of the peak moves to larger times, but its height starts to decrease. The reason for this decrease is likely the same as the one we indicated when we discussed the data for $\phi = 0.50$, i.e., that for large R the system starts to become mean-field like and hence heterogeneities are suppressed.

We also note that the height of the peak is significantly smaller than the one for $\phi = 0.50$. Thus, at large density, steric hindrance dominates and even the faster particles have

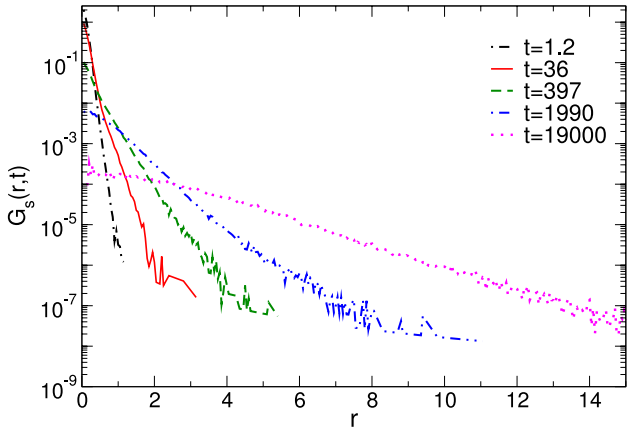

FIG. 13. Self-part of the van Hove function for $R = 2$ and $\phi = 0.70$, parameters for which $\alpha_2(t)$ shows two peaks (see Fig. 12(b)).

less space to move around resulting in significantly less non-Gaussian shapes for $G_s(r,t)$. As a consequence, the dynamics is more homogeneous in this regime compared to the gel at lower ϕ.

To elucidate the origin of the two peaks in the non-Gaussian parameter at $R = 2$, $\phi = 0.70$, we determine how the distribution of particle displacements $G_s(r,t)$ evolves with time. This is shown in Fig. 13. At short times, particle motion is restricted by the local cage of neighbors, and thus, $G_s(r,t)$ is a Gaussian at small r. At larger distances, the distribution has an exponential tail which is due to a few particles that have escaped the steric hindrance cage, in agreement with the usual heterogeneous glassy dynamics in supercooled systems.[4] The presence of these two processes gives rise to the maximum in α_2 at short times. At around $t = 400$, most of the particles have escaped from this steric hindrance cage and thus, the dynamics of the system becomes more homogeneous with $G_s(r,t)$ assuming a Gaussian form and hence α_2 decreases again. But with time, the motion of the particles is again restricted, this time by the bonds which have not yet relaxed. Thus, again $G_s(r,t)$ develops a Gaussian shape (with a larger width, determined by the length of the connecting bonds) and an exponential tail, implying an increase in α_2. Later, the network eventually relaxes, the particles are diffusive and thus α_2 decreases again.

The presence of these two different contributions to the shape of $\alpha_2(t)$ can be further clarified by varying the lifetime of the network, i.e., $\tau_{\rm link}$, and in Fig. 14 we show this for the case $\phi = 0.65, R = 6$. Since we scan a large span of time scales and α_2 changes strongly, the data are shown in logarithmic scales. For $\tau_{\rm link} = 1$, we see only a small peak at $t \approx 10$, which corresponds to the one due to the steric hindrance. For $\tau_{\rm link} = 10^2$, we find that this peak has increased a bit in height and its location has also shifted to $t \approx 30$. This change is a consequence of the increased effective coupling between the particles due to the increased lifetime of the bonds. In addition, we see the development of a new (weak) peak at $t \approx 10^3$, which is caused by the network renewal process. Now, if we increase $\tau_{\rm link}$ further, the location of the first peak remains at the same place, since the local crowding effects are unaffected by the network dynamics. In contrast to this, the location of the second peak

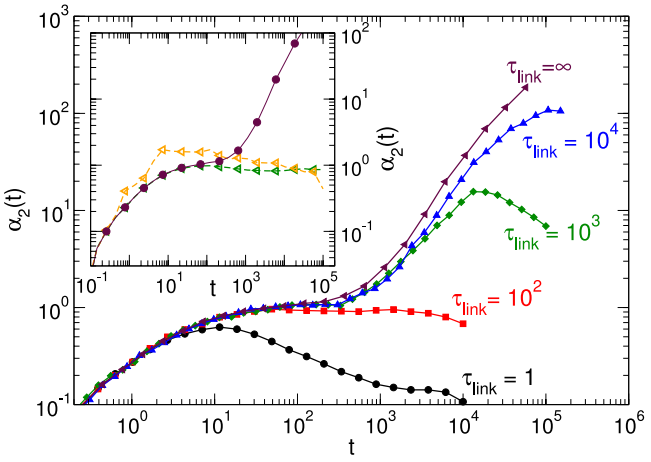

FIG. 14. Time dependence of α_2 for different values of τ_{link} at $R = 6$, $\phi = 0.65$. Inset: for the case of fixed bonds ($\tau_{link} = \infty$), α_2 for the full system (maroon) along with those for the clustered (green open symbols) and non-clustered particles (orange filled symbols).

shifts to longer time scales and its height increases strongly. Since the position of this peak scales with τ_{link}, we recognize that this peak is related to the renewal process. Finally, if we take the case of permanent bonds between the particles, the curve is nearly identical to that for $\tau_{link} = 10^4$, except that we see no signature of it eventually decreasing with time. The reason for these runaway effects is the fact that with increasing lifetime of the network, the unattached particles diffuse away and travel long distances before the network is again renewed. This results in very long extended tails in $G_s(r,t)$, which shows up as very large values for the non-Gaussian parameter. For the case that τ_{link} diverges, the dynamics never becomes Gaussian and $\alpha_2(t)$ diverges at long times.

It is interesting that if one computes, for $\tau_{link} = \infty$, $\alpha_2(t)$ separately for the clustered and non-clustered particles, only the peak at short times is observed, i.e., the one which is due to the crowding effects. This is shown in the inset of Fig. 14 for the case of the system of particles where there is a permanently frozen percolating cluster and few unattached particles. In this case, the $\alpha_2(t)$ for the clustered particles follows the curve for the full system, shows the bump at short times, and becomes at long times a constant (see the corresponding data for $\Delta^2(t)$ in Fig. 9). The result that at long times $\alpha_2(t)$ does not go to zero, as it would be the case for vibrations in a typical amorphous solid with $R = 0$, is related to the fact that the spanning cluster is a disordered network of particles that have different local environments. Thus, the large variety of slow floppy motions, related to the slow relaxation in $F_s(q,t)$ over long times (see Fig. 9), gives a non-Gaussian shape for $G_s(r,t)$ even at very long times. This non-Gaussianity is also the reason for the exponential shape of $f_q^{PN}(q)$, as observed earlier, see Fig. 8. For the non-clustered particles, $\alpha_2(t)$ does show a slight decrease beyond the short-time maximum which shows that the relaxation dynamics starts to become a bit more homogeneous. However, it cannot be expected that the non-Gaussian parameter will go to zero even at very long times, since the mobile clusters do have a spread in size and hence a different diffusion constant.

B. Four point susceptibility $\chi_4(q, t)$

We conclude by measuring to what extent the observed heterogeneous dynamics is related to a correlated motion of the particles. This can be quantified by $\chi_4(q,t)$, defined above, measured for $q = 6.0$, i.e., we look for relaxations over distances which are slightly larger than the average particle diameter.

To have a reference, we consider first the case $R = 0$, i.e., when there are no polymers and the system is just a standard glass-forming system. The time dependence of $\chi_4(q,t)$ is shown in Fig. 15(a) for different packing fractions. In agreement with earlier studies on similar systems, Ref. 51, we find that $\chi_4(q,t)$ shows a maximum at a time t that increases with ϕ and which tracks the increasing relaxation time τ_{SH}. The fact that the height of the peak increases with increasing ϕ indicates that the relaxation dynamics become more cooperative, also this in agreement with previous studies for other glass-forming systems.[54]

Next, we contrast this behavior with the case of increasing gelation, i.e., we fix a volume fraction and increase the number of polymer bonds. For this, we choose $\phi = 0.70$, i.e., the same packing fraction for which we have studied the correlation functions and the non-Gaussian parameter, since for this ϕ the effects due to the steric hindrance as well as the network constraints are clearly observed. The corresponding $\chi_4(q,t)$ is shown in Fig. 15(b) for $\tau_{link} = 10^2$. For $0 < R \leq 6$, the location of the peak in $\chi_4(q,t)$ shifts to larger times and the height of the maximum increases. Thus, this trend follows the behavior observed in the data for $F_s(q,t)$ as well as $\alpha_2(t)$, indicating that steric hindrance dominates the relaxation process and that the dynamics becomes more and more collective. However, for $R > 6$, the peak height decreases again and its location becomes independent of R. We can thus conclude that in this regime the relaxation dynamics becomes less cooperative, a result that makes sense since the rewiring of the network is not really a collective process. This result is also in qualitative agreement with the decrease of the maximum in $\alpha_2(t)$, see Fig. 12(b), which showed that the dynamics becomes more homogeneous.

We conclude by investigating how the lifetime of the network-bonds influences the function $\chi_4(q,t)$. For this, we have calculated this observable for the case $\phi = 0.65$ and $R = 6$, i.e., at intermediate density and in the gel phase for which one sees a significant τ_{link}-dependence in the relaxation behavior (see Fig. 7(b)). We see, Fig. 15(c), that at small and intermediate τ_{link}, the location of the peak in $\chi_4(q,t)$ moves to larger time and that its height increases somewhat, i.e., a behavior that is directly related to the steric hindrance mechanism in which the effective cage becomes stiffer due to the increased lifetime of the bonds. However, once τ_{link} exceeds 10^4, we see that $\chi_4(q,t)$ no longer depends on this lifetime, i.e., the rewiring of the network no longer affects the cooperativity of the dynamics and the latter is solely dependent on the steric hindrance.

To end this section, we contrast our results with the ongoing discussion on whether the non-Gaussian parameter $\alpha_2(t)$ and the four-point dynamic susceptibility $\chi_4(t)$ probe the same time scales for dynamic heterogeneity in relaxation.[57,58] It

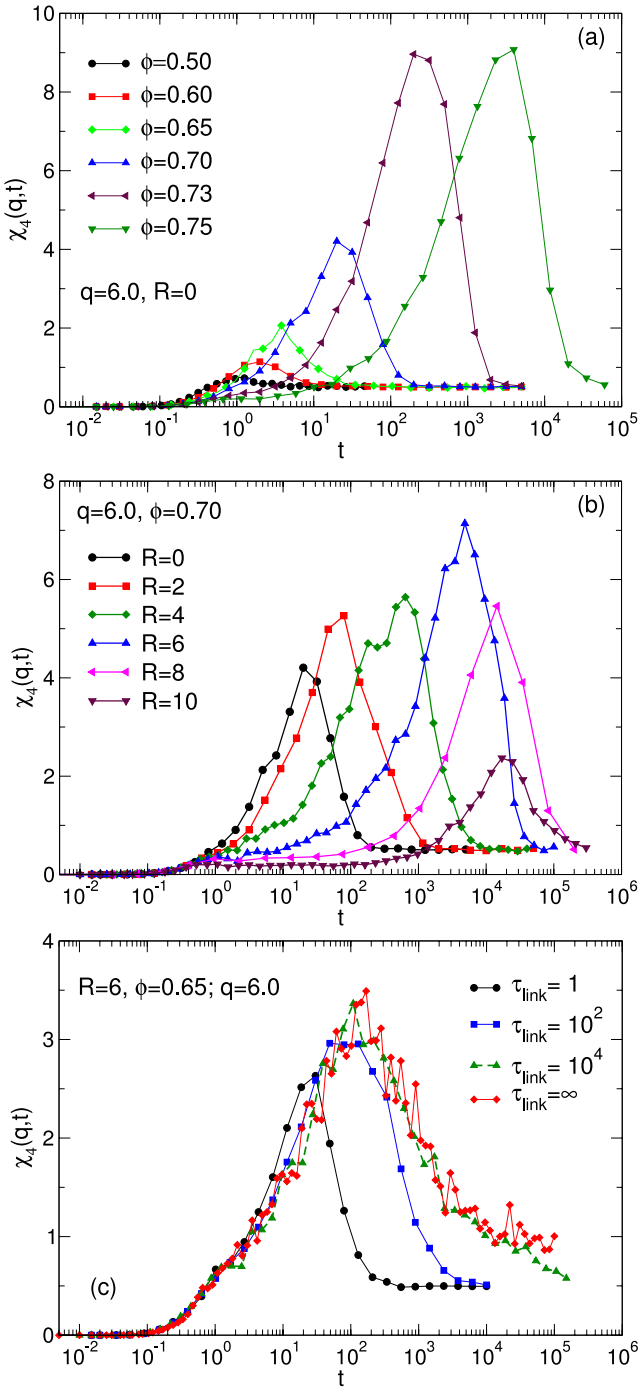

FIG. 15. Time dependence of χ_4 for $\tau_{\rm link} = 100$. (a) $R = 0$ and different values of ϕ. (b) $\phi = 0.70$ and different values of R (as marked on plot). (c) $R = 4$, $\phi = 0.65$ for different values of $\tau_{\rm link}$ (as marked on plot).

has been recently suggested, by analyzing data from model polymer melts, that indeed this is not the case,[57] and similar behavior has been reported in hard-sphere glass-formers.[58] In our case, the distinct behaviour for both quantities stems from the fact that our model displays two different arrest mechanisms in competition, whereas these other studies[57,58] discuss the different case where only steric hindrance is present.

VII. SUMMARY AND CONCLUSIONS

In this paper, we have studied a coarse-grained model for a transient network fluid, a system that can be realized in experiments by an oil-in-water emulsion. By tuning the volume fraction ϕ of the constituent particles, the number of bonds R between the mesoparticle, and the lifetime $\tau_{\rm link}$ of these connections, we have scanned across the phase diagram to investigate the relaxation dynamics of this system, in particular the interplay between the gel-transition and the glass transition induced by steric hindrance effects.

By analyzing the mean-squared displacement and self-intermediate scattering function, we find that the nature of the slowing down depends on the packing fraction: At low ϕ an increase of R leads to a two step relaxation with a plateau that increases continuously with R and an $\alpha-$ relaxation time that is independent of R and that is related to the lifetime of the bonds. In contrast to this, we find at large ϕ a two step relaxation with a plateau height that is basically independent of R whereas the relaxation time does depend on the density of bonds. Thus, these two different behaviors show that the system can show a glassy dynamics that is related on one hand to a gel transition and on the other hand to a glass transition associated with the steric hindrance mechanism. For intermediate densities and a certain range of R and $\tau_{\rm link}$, the interplay between these two mechanisms leads to a decay of the time correlation function that is logarithmic over several decades in time, whereas for other combinations it gives rise to a three step relaxation. We note here that a similar multistep relaxation pattern has been recently reported for mixtures of *multiarm* telechelic polymers and oil-in-water microemulsions,[59] suggesting the existence of a competition of different arrest length- and time-scales in these systems. We have also studied how the height of the plateau at long times, i.e., the Debye-Waller factor, depends on the wave-vector and found that it decays in an exponential manner in q, i.e., very different from the Gaussian decay observed in more standard glass-forming systems.

Furthermore, we have determined the relaxation times of the system and found that these can approximately be factorized into a function that depends strongly on R and a Vogel-Fulcher type dependence on ϕ. The $R-$dependent factor shows for $R \leq 10$ a strong exponential dependence that is related to the escape of the particles from the local cage, whereas for larger values of R the dependence is weaker and linked to an Arrhenius-like process for bond-breaking.

By studying the non-Gaussian parameter we have probed to what extent the relaxation dynamics of the system is heterogeneous. At low packing fraction this dynamics becomes extremely heterogeneous, if R is not too large, since some of the particles are very strongly connected to their neighbors (and hence are immobile) whereas others can move almost freely. However, if R becomes larger than 6, the relaxation dynamics becomes again quite homogeneous since at any time all particles are well connected to their neighbors. At large packing fractions the non-Gaussian parameter shows a double peak structure and, by monitoring the van Hove function, we can show that this feature is directly related to the two relaxation processes, i.e., the steric hindrance and the connectivity of the network.

Whether or not the relaxation dynamics is cooperative can be characterized by the four-point correlation function $\chi_4(q,t)$. We find that for large packing fractions the height of the peak in $\chi_4(q,t)$ increases rapidly with R, showing that the strengthened

coupling leads to an enhanced cooperative motion. However, if R is increased beyond 6, this cooperativity decreases again, since the relaxation dynamics is strongly dominated by the rewiring of the network, i.e., a non-cooperative process.

Summarizing, we see that the interplay between the two different mechanisms giving rise to glassy behavior can lead a rather complex and unusual relaxation dynamics. In the present study, we have focused on a system in which the particles are connected by polymers having a fixed extension length $\ell = 3.5\sigma$. For much smaller extension lengths, one can expect to recover the re-entrant scenario observed in colloidal gels.[7] For longer extension lengths, the particles will instead have more space to explore and it will likely result in an even more floppy network. In the future, it would certainly be worthwhile to explore also systems that have polymers with different values of ℓ, since this implies multiple localization lengths and thus provides novel relaxation scenarios that can subsequently also be studied in experiments. And finally, we recall that our model is motivated by an experimental system which has highly nontrivial rheological properties, e.g., this material flows like a liquid but eventually breaks as a brittle solid,[60,61] being capable of self-healing through thermal fluctuations. Thus, in the future we plan to study the rheological properties of our model in order to understand the microscopic mechanisms that lead to the experimental observations.

ACKNOWLEDGMENTS

Financial support from ANR's TSANET is acknowledged. P.I.H. acknowledges financial support from Spanish MICINN project FIS2009-08451, FIS2013-43201-P, University of Granada, Junta de Andalucía projects P06-FQM1505, P09-FQM4682, and GENIL PYR-2014-13 project. W.K. is member of the Institut Universitaire de France.

[1]K. Binder and W. Kob, *Glassy Materials and Disordered Solids* (World Scientific, Singapore, 2005).
[2]T. A. Witten, *Structured Fluids* (Oxford University Press, Oxford, 2004).
[3]F. Sciortino and P. Tartaglia, Adv. Phys. **54**, 471 (2005).
[4]P. Chaudhuri, L. Berthier, and W. Kob, Phys. Rev. Lett. **99**, 060604 (2007).
[5]V. Lubchenko and P. G. Wolynes, Annu. Rev. Phys. Chem. **58**, 235 (2007).
[6]R. G. Larson, *The Structure and Rheology of Complex Fluids* (Oxford University Press, USA, 1999).
[7]E. Zaccarelli, J. Phys.: Condens. Matter **19**, 323101 (2007).
[8]P. M. Goldbart, H. E. Castillo, and A. Zippelius, Adv. Phys. **45**, 393 (1996).
[9]X. Mao, P. M. Goldbart, X. Xing, and A. Zippelius, Phys. Rev. E **80**, 031140 (2009).
[10]E. Del Gado, A. Fierro, L. de Arcangelis, and A. Coniglio, Phys. Rev. E **69**, 051103 (2004).
[11]P. J. Lu, E. Zaccarelli, F. Ciulla, A. B. Schofield, F. Sciortino, and D. A. Weitz, Nature **453**, 499 (2008).
[12]C. P. Royall, S. R. Williams, T. Ohtsuka, and H. Tanaka, Nat. Mater. **7**, 556 (2008).
[13]C. P. Royall and A. Malins, Faraday Discuss. **158**, 301 (2012).
[14]C. L. Klix, C. P. Royall, and H. Tanaka, Phys. Rev. Lett. **104**, 165702 (2010).
[15]V. Testard, L. Berthier, and W. Kob, Phys. Rev. Lett. **106**, 125702 (2011).
[16]M. Suarez, N. Kern, E. Pitard, and W. Kob, J. Chem. Phys. **130**, 194904 (2009).
[17]P. I. Hurtado, L. Berthier, and W. Kob, Phys. Rev. Lett. **98**, 135503 (2007).
[18]E. Michel, M. Filali, R. Aznar, G. Porte, and J. Appell, Langmuir **16**, 8702 (2000).
[19]P. I. Hurtado, P. Chaudhuri, L. Berthier, and W. Kob, AIP Conf. Proc. **1091**, 166 (2009).
[20]P. Chaudhuri, L. Berthier, P. I. Hurtado, and W. Kob, Phys. Rev. E **81**, 040502(R) (2010).
[21]S. Saw, N. L. Ellegaard, W. Kob, and S. Sastry, Phys. Rev. Lett. **103**, 248305 (2009); J. Chem. Phys. **134**, 164506 (2011).
[22]E. Del Gado and W. Kob, Phys. Rev. Lett. **98**, 028303 (2007).
[23]A. de Candia, E. Del Gado, A. Fierro, and A. Coniglio, J. Stat. Mech. **2009**, 02052.
[24]M. Miller, R. Blaak, C. N. Lumb, and J. P. Hansen, J. Chem. Phys. **130**, 114507 (2009).
[25]E. Zaccarelli, S. V. Buldyrev, E. La Nave, A. J. Moreno, I. Saika-Voivod, F. Sciortino, and P. Tartaglia, Phys. Rev. Lett. **94**, 218301 (2005).
[26]F. Sciortino and E. Zaccarelli, Curr. Opin. Solid State Mater. Sci. **15**, 246 (2011).
[27]E. Zaccarelli, I. Saika-Voivod, S. V. Buldyrev, A. J. Moreno, P. Tartaglia, and F. Sciortino, J. Chem. Phys. **124**, 124908 (2006).
[28]E. Zaccarelli and W. C. K. Poon, Proc. Natl. Acad. Sci. U. S. A. **106**, 15203 (2009).
[29]A. M. Puertas, M. Fuchs, and M. E. Cates, Phys. Rev. Lett. **88**, 098301 (2002).
[30]M. Lagi, P. Baglioni, and S.-H. Chen, Phys. Rev. Lett. **103**, 108102 (2009).
[31]A. Duri and L. Cipelletti, EPL **76**, 972 (2006).
[32]J. Bergenholtz and M. Fuchs, Phys. Rev. E **59**, 5706 (1999).
[33]K. Dawson, G. Foffi, M. Fuchs, W. Götze, F. Sciortino, M. Sperl, P. Tartaglia, T. Voigtmann, and E. Zaccarelli, Phys. Rev. E **63**, 011401 (2000).
[34]K. Kroy, M. E. Cates, and W. C. K. Poon, Phys. Rev. Lett. **92**, 148302 (2004).
[35]C. Zhao, G. Yuan, and C. C. Han, Soft Matter **10**, 8905 (2014).
[36]I. Hoffmann, P. M. de Molina, B. Farago, P. Falus, C. Herfurth, A. Laschewsky, and M. Gradzielski, J. Chem. Phys. **140**, 034902 (2014).
[37]C. P. Royall, S. R. Williams, and H. Tanaka, "The nature of the glass and gel transitions in sticky spheres," e-print arXiv:1409.5469.
[38]A. J. Moreno and J. Colmenero, Phys. Rev. E **74**, 021409 (2006).
[39]M. Sperl, E. Zaccarelli, F. Sciortino, P. Kumar, and H. E. Stanley, Phys. Rev. Lett. **104**, 145701 (2010).
[40]A. M. Puertas and M. Fuchs, in *Structure and Functional Properties of Colloidal Systems*, edited by R. Hidalgo-Alvarez (Taylor and Francis, London, 2009).
[41]M. Bernabei, A. J. Moreno, and J. Colmenero, Phys. Rev. Lett. **101**, 255701 (2008).
[42]N. Khalil, A. de Candia, A. Fierro, M. P. Ciamarra, and A. Coniglio, Soft Matter **10**, 4800 (2014).
[43]H. Furukawa, Adv. Phys. **34**, 703 (1985).
[44]Note that the full inter-particle potential, with our choice of $\epsilon_2 = 50$, see Eq. (1), has a minimum at around 1σ, see Fig. 1 in Ref. 19, which therefore determines the characteristic localization length due to the bonds, see dashed line in Fig. 3(b).
[45]W. Kob and H. C. Andersen, Phys. Rev. E **51**, 4626 (1995).
[46]M. Nauroth and W. Kob, Phys. Rev. E **55**, 657 (1997).
[47]A. M. Puertas, M. Fuchs, and M. E. Cates, Phys. Rev. E **67**, 031406 (2003).
[48]K. Kim, K. Miyazaki, and S. Saito, EPL **88**, 36002 (2009).
[49]J. Kurzidim, D. Coslovich, and G. Kahl, Phys. Rev. Lett. **103**, 138303 (2009).
[50]W. Kob, C. Donati, S. J. Plimpton, P. H. Poole, and S. C. Glotzer, Phys. Rev. Lett. **79**, 2827 (1997).
[51]N. Lacevic, F. W. Starr, T. B. Schroder, and S. C. Glotzer, J. Chem. Phys. **119**, 7372 (2003).
[52]I. Saika-Voivod, H. M. King, P. Tartaglia, F. Sciortino, and E. Zaccarelli, J. Phys.: Condens. Matter **23**, 285101 (2011).
[53]C. De Michele, S. Gabrielli, P. Tartaglia, and F. Sciortino, J. Phys. Chem. B **110**, 8064 (2006).
[54]C. Toninelli, M. Wyart, L. Berthier, G. Biroli, and J.-P. Bouchaud, Phys. Rev. E **71**, 041505 (2005).
[55]T. Abete, A. de Candia, E. Del Gado, A. Fierro, and A. Coniglio, Phys. Rev. E **78**, 041404 (2008).
[56]J. Colombo and E. Del Gado, Soft Matter **10**, 4003 (2014).
[57]F. W. Starr, J. F. Douglas, and S. Sastry, J. Chem. Phys. **138**, 12A541 (2013).
[58]A. J. Dunleavy, K. Wiesner, R. Yamamoto, and C. P. Royall, Nat. Commun. **6**, 6089 (2015).
[59]P. Malo de Molina, C. Herfurth, A. Laschewsky, and M. Gradzielski, Langmuir **28**, 15994 (2012).
[60]H. Tabuteau, S. Mora, G. Porte, M. Abkarian, and C. Ligoure, Phys. Rev. Lett. **102**, 155501 (2009).
[61]C. Ligoure and S. Mora, Rheol. Acta **52**, 91 (2013).